

Article

Mini-Beam Spatially Fractionated Radiation Therapy for Whole-Brain Re-Irradiation—A Pilot Toxicity Study in a Healthy Mouse Model

Hong Yuan ^{1,2,*} , Judith N. Rivera ^{3,4}, Jonathan E. Frank ², Jonathan Nagel ⁵, Colette Shen ⁶ 
and Sha X. Chang ^{3,6,*} 

¹ Department of Radiology, University of North Carolina at Chapel Hill, Chapel Hill, NC 27599, USA

² Biomedical Research Imaging Center, University of North Carolina at Chapel Hill, Chapel Hill, NC 27599, USA

³ Joint Department of Biomedical Engineering, University of North Carolina at Chapel Hill, Chapel Hill, NC 27599, USA

⁴ Department of Radiation Oncology, Indiana University Health, Indianapolis, IN 46202, USA

⁵ Department of Pathology and Lab Medicine, University of North Carolina at Chapel Hill, Chapel Hill, NC 27599, USA

⁶ Department of Radiation Oncology, University of North Carolina at Chapel Hill, Chapel Hill, NC 27599, USA

* Correspondence: yuanh@med.unc.edu (H.Y.); sha_chang@med.unc.edu (S.X.C.)

Simple Summary: Finding a safer and more effective treatment for patients with recurrent brain metastases is a pressing medical need. The study explored a mini-beam radiotherapy (MBRT), a type of spatially fractionated radiation therapy, in a healthy mouse model for whole-brain re-irradiation. Radiation toxicity was evaluated with three re-irradiation schemes: uniform radiation, low-dose MBRT, and high-dose MBRT. The results showed that the low-dose MBRT group experienced less body weight loss and had more progenitor cells preserved in brain compared to both uniform radiation and high-dose MBRT. The study suggests that MBRT at an appropriate dose level may be a safer option for whole-brain re-irradiation.



Citation: Yuan, H.; Rivera, J.N.; Frank, J.E.; Nagel, J.; Shen, C.; Chang, S.X. Mini-Beam Spatially Fractionated Radiation Therapy for Whole-Brain Re-Irradiation—A Pilot Toxicity Study in a Healthy Mouse Model. *Radiation* **2024**, *4*, 125–141. <https://doi.org/10.3390/radiation4020010>

Academic Editor: Gabriele Multhoff

Received: 8 February 2024

Revised: 22 April 2024

Accepted: 30 April 2024

Published: 8 May 2024



Copyright: © 2024 by the authors. Licensee MDPI, Basel, Switzerland. This article is an open access article distributed under the terms and conditions of the Creative Commons Attribution (CC BY) license (<https://creativecommons.org/licenses/by/4.0/>).

Abstract: For patients with recurrent brain metastases, there is an urgent need for a more effective and less toxic treatment approach. Accumulating evidence has shown that spatially fractionated radiation therapy (SFRT) is able to provide a significantly higher therapeutic ratio with lower toxicity compared to conventional radiation using a uniform dose. The purpose of this study was to explore the potential low toxicity benefit of mini-beam radiotherapy (MBRT), a form of SFRT, for whole-brain re-irradiation in a healthy mouse model. Animals first received an initial 25 Gy of uniform whole-brain irradiation. Five weeks later, they were randomized into three groups to receive three different re-irradiation treatments as follows: (1) uniform irradiation at 25 Gy; (2) MBRT at a 25 Gy volume-averaged dose (106.1/8.8 Gy for peak/valley dose, 25 Gy-MBRT); and (3) MBRT at a 43 Gy volume-averaged dose (182.5/15.1 Gy for peak/valley dose, 43 Gy-MBRT). Animal survival and changes in body weight were monitored for signs of toxicity. Brains were harvested at 5 weeks after re-irradiation for histologic evaluation and immunostaining. The study showed that 25 Gy-MBRT resulted in significantly less body weight loss than 25 Gy uniform irradiation in whole-brain re-irradiation. Mice in the 25 Gy-MBRT group had a higher level of CD11b-stained microglia but also maintained more Ki67-stained proliferative progenitor cells in the brain compared to mice in the uniform irradiation group. However, the high-dose 43 Gy-MBRT group showed severe radiation toxicity compared to the low-dose 25 Gy-MBRT and uniform irradiation groups, indicating dose-dependent toxicity. Our study demonstrates that MBRT at an appropriate dose level has the potential to provide less toxic whole-brain re-irradiation. Future studies investigating the use of MBRT for brain metastases are warranted.

Keywords: spatially fractionated radiation therapy; mini-beam radiotherapy; whole-brain re-irradiation; radiation toxicity

1. Introduction

Brain metastases occur in 10–30% of cancer patients, and the incidence has been increasing over the past two decades [1,2]. As patients are living longer because of improvements in systemic and local therapy, there is an increased possibility for patients to develop additional brain metastases after initial treatment [3,4]. While stereotactic radiosurgery (SRS) is increasingly used for patients with small and limited numbers of brain metastases, whole-brain radiotherapy (WBRT) is still the standard of care for patients presenting with multiple brain metastases [1,2,5]. Even after successful treatment, brain metastases often recur. Salvage radiotherapy after prior WBRT is one of the treatment options. Whole-brain re-irradiation after prior WBRT has been evaluated in several studies and has shown some improvements in neurological symptoms in patients with brain metastases [6–9]. However, the neurotoxicity and cognitive effects of repeat WBRT are a major concern [10]. In an era of increasing survival with metastatic disease, there is a significant unmet need for better re-irradiation approaches that can provide effective tumor control while minimizing short- and long-term treatment toxicity.

Spatially fractionated radiation therapy (SFRT) is a non-conventional form of radiation therapy that is characterized by the coexistence of both high and low-dose regions within the treatment volume, often using a single or few fraction treatments [11,12]. Preclinical SFRT research using the form of microbeam radiation therapy (MRT) [13] has demonstrated a very high therapeutic ratio with improved survival in a rat gliosarcoma model after MRT (peak dose of 400 Gy, valley dose of 17.9 Gy) compared to conventional uniform radiation (17.9 Gy) [14], and “unusual resistance to necrosis” of the rat brain to MRT with peak doses as high as 625 Gy [15]. In recent years, mini-beam radiation therapy (MBRT) using larger spatial fractionation scales on the order of millimeters instead of the tens of microns used in classical MRT [16,17] has been established as another form of SFRT [18–20]. In our previous study, we demonstrated that MBRT has normal tissue-sparing effects with a peak dose of either 48 Gy or 72 Gy in mouse brains inoculated with U87 brain tumors [21]. Ionizing radiation photons or particles have the physical ability to generate free radicals that may cause direct or indirect DNA damage in common, as well as subcellular changes [22]. Through the combination of DNA damage and subcellular alterations, radiation has the capacity to alter the tumor/tissue microenvironment, cellular architecture, vascular permeability, and cytokine expression, leading to tumor inhibition or normal tissue damage. The mechanisms of how SFRT works differently than conventional radiation and provides a high therapeutic ratio have not been fully elucidated yet. Radiobiological studies conducted so far suggest that the high therapeutic ratio and normal tissue-sparing effects in SFRT might come from a mixed contribution of radiation-induced bystander and abscopal effects, immunologic interactions, as well as vascular and normal tissue repairing in the low-dose valley regions [23–25]. Studies have shown that SFRT can induce a greater antitumor immune response compared to conventional uniform radiotherapy [26]. It is also postulated that the normal cells in the low-dose valley region can migrate and mediate the repair of radiation-damaged tissue efficiently, which may manifest as a normal tissue-sparing effect in SFRT [23]. The exact mechanisms are still under active investigation.

There are many studies evaluating the benefits of SFRT in brain tumor treatment. However, few studies have been focused on the use of SFRT as a re-irradiation option in the management of brain metastases. We hypothesize that MBRT may be superior to conventional uniform radiation with less treatment toxicity as a re-irradiation approach after prior WBRT. To this end, we conducted a pilot preclinical study to compare the treatment toxicity of whole-brain re-irradiation between MBRT and conventional broad beam radiation therapy (BBRT) in non-tumor-bearing healthy mice. Toxicity was evaluated by

changes in body weight, survival, magnetic resonance imaging (MRI), and histopathologic findings. If this hypothesis is confirmed, we can investigate the potential benefit of MBRT re-irradiation on tumor-bearing animals to further explore the local control and therapeutic ratio benefits of SFRT as an approach to whole-brain re-irradiation.

2. Materials and Methods

2.1. Study Design

The experimental study design is shown in Figure 1. Healthy normal mice were used in this study to evaluate the radiation toxicity. All animals received an initial whole-brain irradiation of 25 Gy using conventional WBRT, followed by re-irradiation 5 weeks later. After the initial WBRT radiation, the mice were divided into three re-irradiation treatment groups: 25 Gy conventional broad beam radiation (25 Gy-BBRT), mini-beam radiation with the same volume-averaged dose of 25 Gy (25 Gy-MBRT), and a higher dose mini-beam radiation with a volume-averaged dose of 43 Gy (43 Gy-MBRT). The 25 Gy-MBRT group had peak and valley doses of 106.1 Gy and 8.8 Gy, respectively. The 43 Gy-MBRT group had peak and valley doses of 182.5 Gy and 15.1 Gy, respectively. The details are shown in Table 1. Valley dose is considered to be a key dosimetric parameter associated with MRT brain toxicity, and it is kept below the conventional uniform beam tolerance dose level to avoid toxicity [27,28]. The 15 Gy valley dose in the 43 Gy-MBRT group was used in this study to determine whether it resulted in toxicity between the 8.8 Gy valley dose in the 25 Gy-MBRT group and the 25 Gy uniform radiation dose in the 25 Gy-BBRT group for whole-brain re-irradiation.

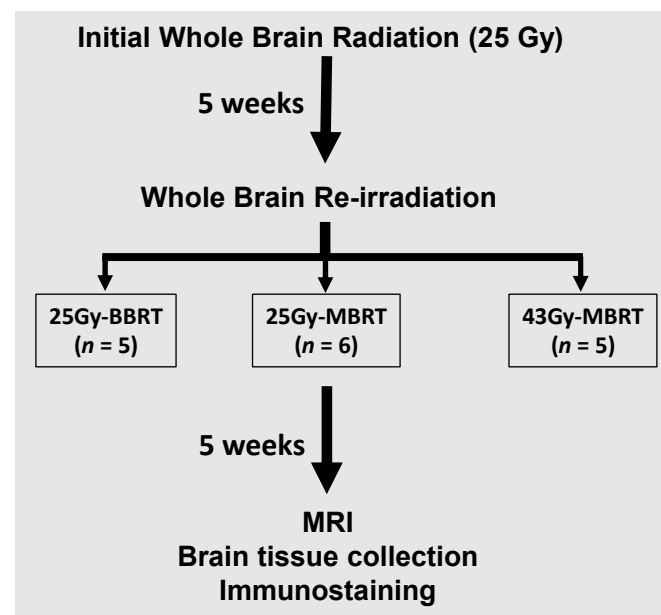


Figure 1. Design of the whole-brain re-irradiation study.

Animal body weight and survival were monitored and recorded throughout the study. Animals were euthanized when reaching humane endpoints, and days of survival were recorded. The study was terminated at 5 weeks after re-irradiation, and all remaining surviving animals were ethically euthanized and brain tissue harvested for histological analysis. In addition, a subset of animals underwent MRI brain scans one day prior to brain harvesting.

Table 1. Dosimetry parameters of whole-brain re-irradiation.

Treatment Group	# of Animals	Vol-Avg Dose ^{a,b} (Gy)	Peak Dose ^{a,b} (Gy)	Valley Dose ^{a,b} (Gy)	PVDR	Valley Width (mm)	Peak Width (mm)	% Volume Directly Irradiated
25 Gy-BBRT	5	25	27	27	1	NA	NA	100
25 Gy-MBRT	6	25	106.1	8.8	12.1	0.9	0.31	25.6
43 Gy-MBRT	5	43	182.5	15.1	12.1	0.9	0.31	25.6

^a Computed at 5 mm tissue depths except for the vol-avg dose, which was computed within a 10 mm depth.

^b Measurements were determined via a film dosimetry calibrated against the ion chamber.

2.2. Animal Model

Seventeen female C57BL/6 mice (6~7 weeks old) from the Jackson Laboratory were used for the experiments. For both radiation and imaging, the mice were anesthetized using isoflurane inhalation (3% for induction and 1.5% for maintenance) mixed with oxygen. The depth of anesthesia was determined by the animal's respiratory rate and toe pinch reflex. All animals received the initial 25 Gy whole-brain uniform irradiation and were randomly assigned to one of the three treatment groups for re-irradiation. All mice were housed and treated in the same condition except for the difference in re-irradiation.

Animals were carefully monitored daily throughout the study. Body weight was recorded every two days after radiation treatment for two weeks and at least every four days thereafter until the end of the study. Study endpoints included animal weight loss of 30% compared to the pre-treatment animal body weight, body condition scores of equal to or less than 2, or other signs of pain, discomfort, or moribundity, as recommended by the veterinary staff. Animals meeting the humane endpoint criteria were ethically euthanized. All animal procedures were included in the animal protocol approved by the UNC Institutional Animal Care and Use Committee (IACUC).

2.3. Radiation Dosimetry and Treatment

A research irradiator (XRad-320, Precision X-Ray Inc., North Branford, CT, USA) was used for all radiation treatments in this study. X-ray radiation was generated with a peak energy of 320 kV, a current of 12.5 mA, and 0.254 mm copper filtration. A custom-made Cerrobend collimator was used to define a 10 mm × 10 mm radiation field for the 25 Gy BBRT treatment. For the MBRT treatments, a custom-made tungsten mini-beam collimator was used [20]. Radiation dosimetry was performed in a similar manner as that described in our previous work [20]. Briefly, the EBT-3 radiochromic film was calibrated against an ADCL-traced ion chamber under large field conditions in the XRad-320 irradiator. An acrylic mouse-sized phantom was used to measure beam profiles (with the film perpendicular to the radiation beams) and percentage depth dose (PDD) (with the film parallel to the radiation beams) for each radiation field. The results of the film dosimetry are shown in Figure 2. The volume-averaged dose for the whole-brain treatment is computed by averaging the radiation dose within a 10 mm (across the peaks) × 10 mm (depth) area of the PDD film. Radiation dosimetry used in the whole-brain re-irradiation is shown in Table 1, including measurements for the peak dose, valley dose, peak-to-valley dose ratio (PVDR), valley width, peak width, and % volume directly irradiated by the beams. Note that both MBRT treatment groups used the same collimator and, therefore, shared the same spatial profile parameters.

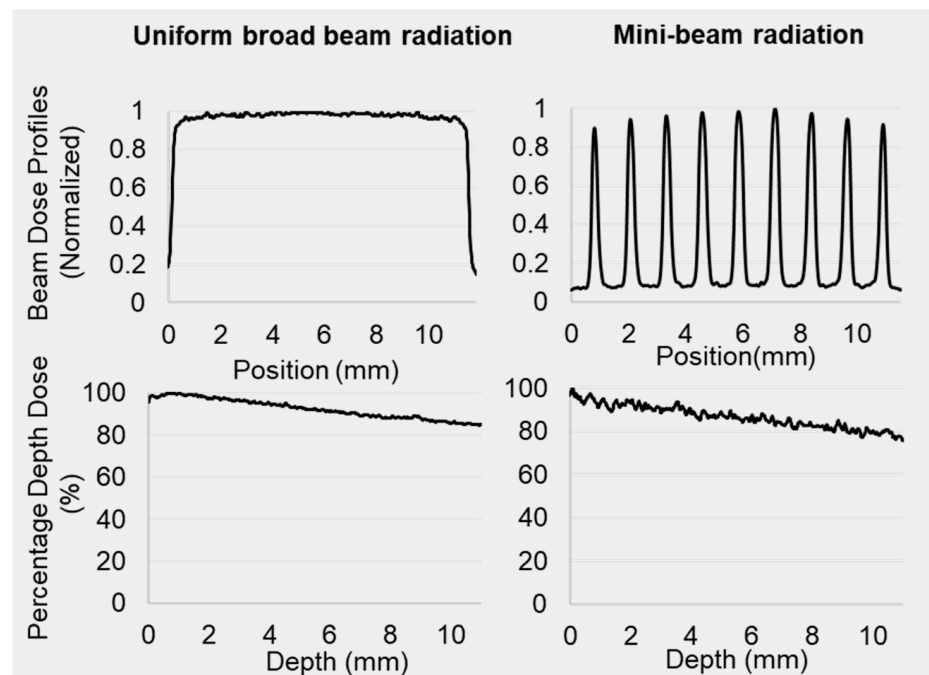


Figure 2. MBRT dose profiles and percentage of depth dose measurements. Beam profiles and percentage depth dose (PDD) for the 25 Gy BBRT and the two MBRT treatments were measured by EBT-3 film calibrated against an ion chamber in large field conditions. The dose rate at the 5 mm tissue depth is 3.5 Gy/min for the mini-beam and 4.98 Gy/min for the broad beam radiation.

The animal irradiation procedure used in this study has been described previously [20]. In this study, both the initial irradiation and the re-irradiation were carried out using the X-rad-320 irradiator. The mice were placed in the left lateral decubitus position (lying on the left side) during irradiation. An effective field size on the animal head is 5 mm (the treatment field is 10 mm × 10 mm with 5 mm skin flash—a field in the air) in the dorsal–ventral direction and 10 mm in the posterior–anterior direction for both the BBRT and MBRT treatments. The alignment of the radiation beam with the mouse anatomy is described in Figure 3. A sagittal view of the mouse head CT is used as a reference for targeting the radiation field to the brain. The yellow outlines in Figure 3B,C represent the radiation field boundaries, and they are defined by the externally visible anatomical markers (eyes, ears, and midline). A PC-linked camera with live video feed was used for radiation–anatomy alignment, using the light field and monitoring animal respiration and motion throughout treatment. Whole-brain radiation targeting was achieved by (1) taping a piece of EBT-3 film over the mouse head facing the radiation beam, (2) delineating the boundaries of the 5 mm × 10 mm radiation field on the film based on the anatomical markers, as described above, (3) placing the animal in the irradiator at the animal positioning station, and (4) aligning the radiation light field with the radiation field markers on the film using the video from the PC-linked camera and the positioning station. The treatment verification film documented the treatment delivery quality. Animals were removed from the study if the verification film showed significant animal motion during treatment delivery or errors in radiation targeting (none occurred in this study).

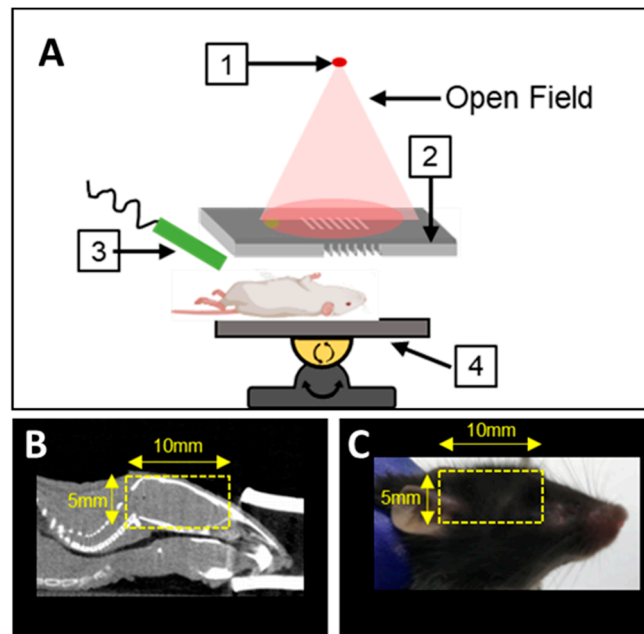


Figure 3. Animal radiation setup. (A) The radiation treatment setup includes (1) an external beam X-ray source, (2) an in-house Cerrobend MBRT or BBRT collimator, (3) a PC-linked camera, which provides a beam's-eye-view of the light field on animals, and (4) an adjustable stage for the animals. (B) Offline CT image used to design the treatment field; (C) Photo of an animal for radiation treatment using the ear and eye as a landmark to position the treatment field during alignment. The 5 mm skin flash above the head (half of the 10 mm × 10 mm field treating air) is not shown.

2.4. MRI Imaging

MR imaging was performed in a subset of mice 5 weeks after brain re-irradiation. All the MRIs were carried out on a preclinical 9.4 Tesla MRI system (BioSpect-94/30 model, Bruker Biospin Corp., Billerica, MA, USA) at the UNC MRI Core Facility. Mice were kept in anesthesia using isoflurane (1.5%) mixed with oxygen during imaging. A phased array surface coil was placed closely right on top of the mouse head. T2-weighted images were acquired using a Rapid Acquisition with Refocused Echoes (RARE) sequence (TE/TR = 22/3400 ms, RARE factor = 8, 0.5 mm slice thickness, and 100 μ m in-plane resolutions). T1-weighted images were acquired using a 2D fast low-angle shot (FLASH) sequence with TE/TR = 3.98/300 ms, flip angle = 30, slice thickness = 0.5 mm, matrix = 150 × 200, and a field of view = 15 × 20 mm. A bolus dose of the gadolinium contrast agent (0.2 mmol/kg, Magnevist[®]) was manually injected through a tail vein catheter. At 15 min post-contrast injection, a T1-weighted MRI was acquired for post-contrast imaging using the exact same protocol as the pre-contrast T1-weighted MRI.

2.5. Immunostaining

At the end of the study (5 weeks after re-irradiation), all brains from the surviving animals were collected for immunofluorescence (IF) staining. All brain tissue was first fixed in 10% buffered formalin for 5 days. The right half of the brain was embedded in paraffin to be sectioned in the sagittal direction. Brain tissue was sectioned to a thickness of 5 microns. Six sections at 2 mm from the midline were collected for further histology and immunohistochemistry analysis. The brain tissue sections were baked and deparaffinized. Histology staining was performed using the standard hematoxylin and eosin (H&E) staining protocol. Immunostaining was carried out in a Leica Bond-III autostainer (Leica Biosystems, Deer Park, IL, USA) to assess microglia activation (CD11b staining) and cell proliferation (Ki67 staining).

For immunofluorescence staining, tissue samples were first processed with antibody retrieval, washing, and blocking for non-specific binding. They were then incubated

with the primary antibodies to CD11b (Abcam, Boston, MA, USA, catalog #ab133357, 1:5000 dilution with incubation for 30 min at room temperature) and Ki67 (Biocare Medical, Pacheco, CA, USA, catalog #CRM325A, 1:50 dilution with incubation for 1 h). Slides were then washed and incubated with the Novolink polymer (Leica Biosystems, Deer Park, IL, USA, catalog # RE7112) as a secondary antibody, followed by linking the fluorophore with either Cyanine 3 (Cy3) or Cyanine 5 (Cy5) and counterstaining with Hoechst 33258 (Invitrogen, Waltham, MA, USA) for the nuclei. Slides were sealed with a coverslip using the ProLong Gold antifade medium, which was scanned in the Aperio Scan Scope FL scanner (Leica Biosystems, Deer Park, IL, USA) for digital fluorescence images.

In CD11b staining images, regions of interest (ROIs) were drawn in the frontal cortex (FC, Cingular area including CG1 and CG2 with about 3 mm anterior-posterior distance), hippocampus (HP), and thalamus (TH) regions in each brain section (2 mm from the midline). Positive-stained cells were segmented in the Cy3 channel using Otsu thresholding algorithms in ImageJ (1.52p version). The area fraction of the CD11b-positive area over each ROI was reported for the FC, HP, and TH region of each animal.

In Ki67 stained images, the same regions were delineated for the frontal cortex, hippocampus, and thalamus in each brain section. The Ki67-positive nuclei were counted in the Cy5 channel, and Hoechst counter-stained total nuclei were counted in the blue channel. The fraction of positively stained cells over the total nuclei number in each region was quantified for each animal.

2.6. Statistical Methods

Survival curves were compared between the three groups and analyzed by the Log-rank test. Differences in body weight changes and immunostaining of CD11b and Ki67 in various brain regions between the 25 Gy-BBRT and 25 Gy-MBRT groups were compared using either Student's *t*-test or the Wilcoxon rank test, assuming equal variances. *p*-values < 0.05 were considered statistically significant. GraphPad Prism software (version 9.0) was used for statistical evaluation.

3. Results

3.1. Gross Assessment, Body Weight Change, and Survival

All animals in this study survived after the initial 25 Gy whole-brain conventional uniform radiation single fraction treatment. The recorded body weight showed that there was an initial weight loss starting on day 4, continuing until day 9, followed by a gradual recovery from initial radiation (Figure 4A). Around day 12 after the initial WBRT treatment, all mice had recovered from body weight loss and had about a 15% body weight increase compared to the baseline. At 5 weeks post the initial WBRT radiation, these mice were randomly divided into three groups for re-irradiation treatment, as described in the Study Design section: 25 Gy-BBRT (*n* = 5), 25 Gy-MBRT (*n* = 6), and 43 Gy-MBRT (*n* = 5) groups. Animal survival days and body weight were monitored after re-irradiation.

Figure 4B shows the Kaplan–Meier survival curves for the three groups. The 43 Gy-MBRT group had the highest mortality, with only one in five animals surviving 5 weeks after re-irradiation. The log-rank test showed no significant differences in survival between the 25 Gy-BBRT and 25 Gy-MBRT groups (*p* = 0.94). However, there were significant differences in body weight and body weight changes between the 25 Gy-BBRT and the 25 Gy-MBRT groups. Note that the same volume average dose of 25 Gy (Table 1) was used for the re-irradiation of these two groups, with the only difference being in the spatial fractionation of the radiation. The mean body weight in the 25 Gy-MBRT group was significantly higher than that in the 25 Gy-BBRT group on day 10 post-re-irradiation (18.8 ± 0.5 vs. 14.0 ± 0.7 , *p* = 0.0004, Student's *t*-test). Body weight changes on day 10 and day 28 post-re-irradiation compared to the start of the re-irradiation are plotted in Figure 4C. When assessed on day 10 post-re-irradiation, mice in the 25 Gy-BBRT group had an average body weight loss of 20.2%. In contrast, mice in the 25 Gy-MBRT group mostly maintained body weight with an average body weight gain of 0.9%. On day 28

post-re-irradiation, mean body weight in the 25 Gy-MBRT group was higher than that of the 25 Gy-BBRT group, although not statistically significant (19.0 ± 1.3 vs. 15.8 ± 0.7 , $p = 0.078$, Student's *t*-test). Mice in the 25 Gy-BBRT group had an average weight loss of 11.4% at 28 days post-re-irradiation, while mice in the 25 Gy-MBRT group had an average body weight gain of 2.1%. Mice in the 43 Gy-MBRT group had an average body weight loss of 20.1% on day 10 with only one mouse, surviving for 28 days post-re-irradiation with the full recovery of body weight loss, indicating severe radiation-induced toxicity in this group. Figure 4D–F shows the changes in body weight of individual animals one month after re-irradiation. Both 25 Gy-BBRT and 43 Gy-MBRT experienced steep body weight loss until day 10 post irradiation. In contrast, the 25 Gy-MBRT group had delayed body weight loss, and the majority maintained their body weight after re-irradiation. Our results suggest that whole-brain re-irradiation with MBRT at the 25 Gy volume-averaged dose may result in less toxicity compared to the same volume-averaged dose of uniform radiation. The results from the two MBRT groups suggest dose-dependent radiation toxicity. Most mice cannot survive a high dose of MBRT with a volume average dose at 43 Gy (peak and valley dose of 182.5 Gy and 15.1 Gy, respectively).

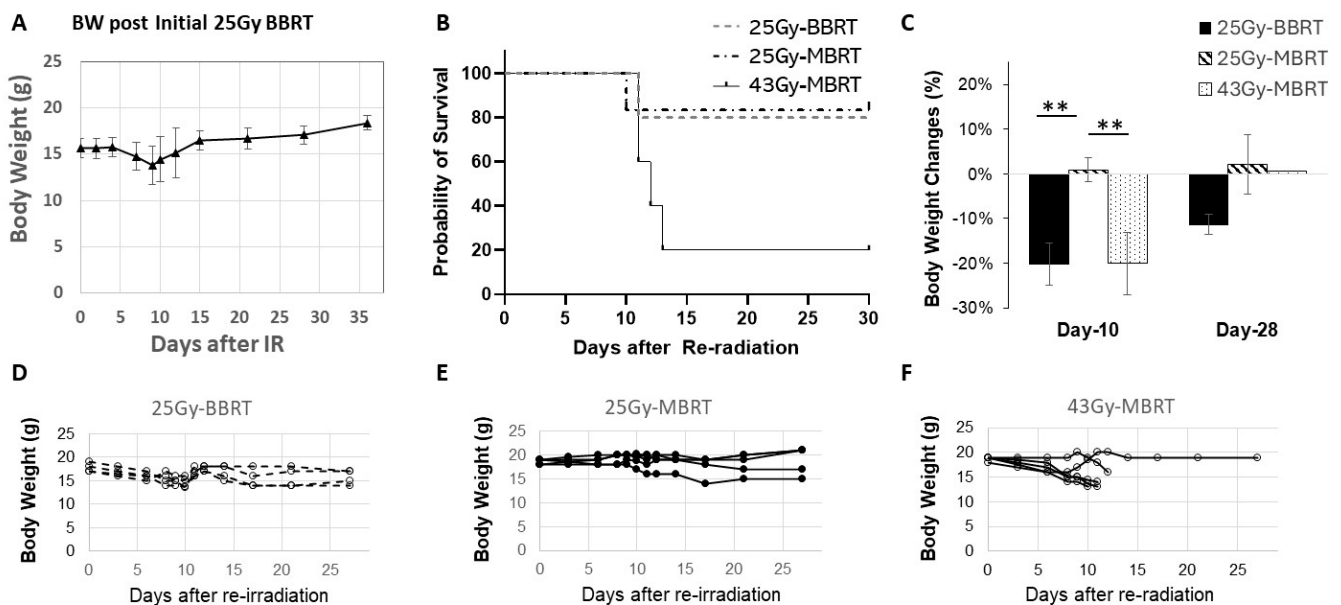


Figure 4. Survival and body weight monitoring. (A) Body weight loss after the initial 25 Gy conventional whole-brain radiation treatment (WBRT). Plot shows the body weight of all mice included in the study (mean and standard deviation) over the first 5 weeks post initial radiation. (B) Kaplan–Meier plot of survival for the three re-irradiation treatment groups. (C) Body weight changes at 10 days and 28 days after re-irradiation treatment for the three groups. The 43 Gy-MBRT group only had one mouse surviving at 28 days; thus, no standard deviation was calculated. Stars (**) indicate $p < 0.001$. (D–F): Body weight monitoring for individual mice (each line represents a single animal) over a month after the re-irradiation for the three groups. Both 25 Gy-BBRT and 43 Gy-MBRT experienced initial steep body weight loss. The 25 Gy-MBRT had delayed body weight loss, and the majority maintained their body weight after re-irradiation.

3.2. MRI Assessment

MR imaging was conducted at the end of the study (5 weeks post-re-irradiation) on five surviving mice ($n = 2$ from 25 Gy-BRT and 25 Gy-MBRT groups, and $n = 1$ from 43 Gy-MBRT group). As shown in Figure 5, the T2-weighted MRI showed no apparent damage. There were no enlarged ventricles and no radiation-induced edema, necrosis, or fibrosis in brain structures among mice from the three groups. Pre- and post-contrast T1-weighted MR images showed no apparent change in contrast enhancement, indicating

no changes in vascular permeability at 5 weeks after re-irradiation in mice from the three groups. The analysis was limited by the number of animals that were imaged.

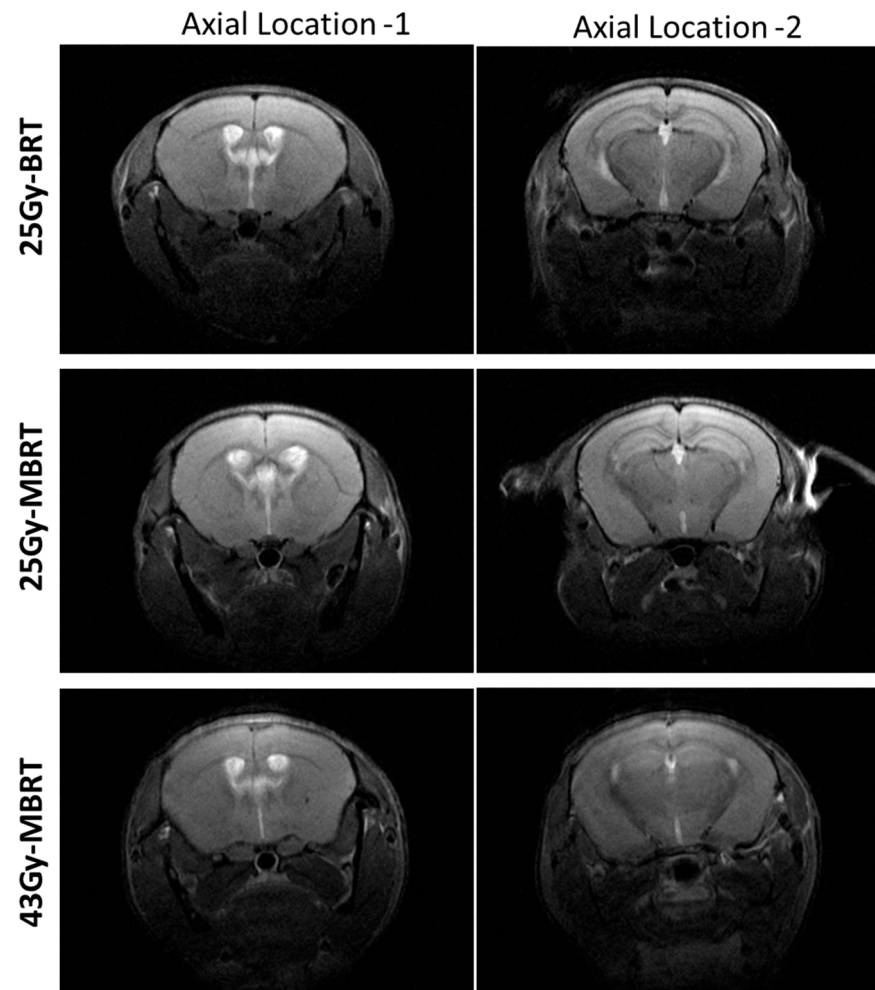


Figure 5. T2-weighted MR images from three treatment groups at 5 weeks post-re-irradiation. Axial location-1 is at 0.1 mm anterior to the bregma, and axial location-2 is at 2.1 mm posterior to the bregma. No significant edema or gross brain tissue damage was found at 5 weeks post-re-irradiation among the surviving mice from the three treatment groups.

3.3. H&E and Immunostaining

Immunohistochemical staining was performed on the surviving mice from the 25 Gy-BBRT group ($n = 4$), 25 Gy-MBRT group ($n = 4$), and 43 Gy-MBRT group ($n = 1$) at 5 weeks post-re-irradiation. Since only one mouse was left from the 43 Gy-MBRT group, the comparison was mainly focused on the 25 Gy-BBRT and 25 Gy-MBRT groups.

H&E staining (Figure 6 upper panel) of brain sections from the 25 Gy-BBRT and 25 Gy-MBRT groups ($n = 4$ for each group) showed mild parenchymal vacuolization in the thalamus, hypothalamus, and brainstem. In the 43 Gy-MBRT mouse, a few scattered necrotic neurons were noted throughout the cerebral cortex, and patchy vacuolization was observed in the hippocampal neuropil. No significant neuronal damage was found in all brain sections 5 weeks after re-irradiation.

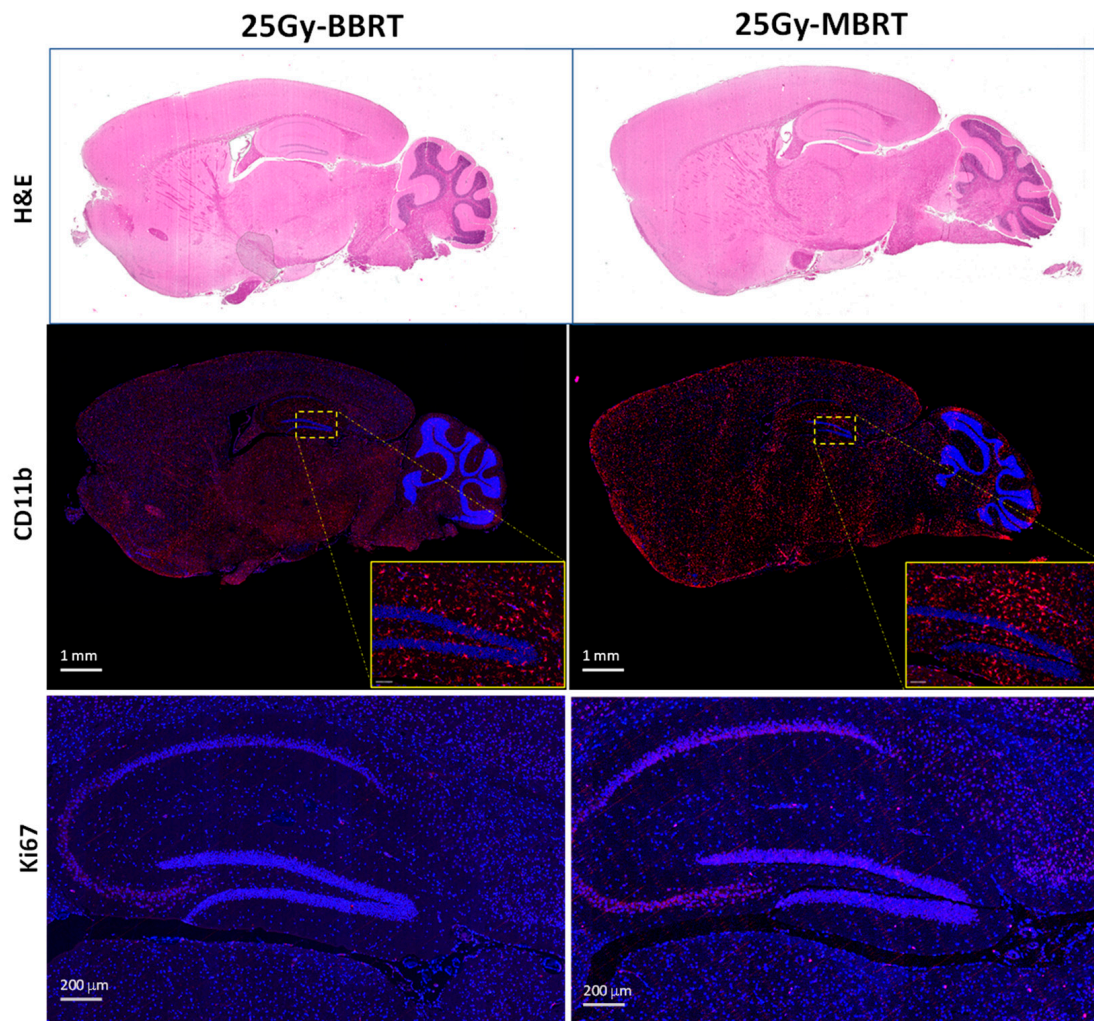


Figure 6. H&E and immunostaining of CD11b and Ki67 in the brain tissue at 5 weeks post-re-irradiation. H&E staining (**top panel**) showed no significant differences in cell morphology between the 25 Gy-BBRT and 25 Gy-MBRT groups. (**Middle panel**) shows CD-11b staining for activated microglia in the irradiated brains from both groups. CD11b staining (red) in brains from the 25 Gy-MBRT group shows high and low expression bands corresponding to the peak (higher expression level) and valley (lower expression level) dose region in MBRT. Brains from the BBRT group shows a more uniform elevated level of microglia. Note that the high staining signal at the edge of the brain section was a staining artifact, as confirmed by high magnification microscopy. (**Lower panel**) shows Ki67 staining in the 25 Gy-BBRT and 25 Gy-MBRT groups. There were much more Ki67-positive cells (red) in the MBRT group compared to those in the BBRT group. The blue channel shows the Hoechst counter stain of nuclei.

CD11b staining (Figure 6 middle panel) was conducted to examine neuroinflammation, as indicated by the staining of activated microglia. There were significantly higher numbers of activated microglia in the brains of all treated groups, as shown in Figure 6. Brains from the BBRT group showed a more uniformly elevated level of activated microglia. In contrast, CD11b staining in brains from the 25 Gy-MBRT group showed high and low staining bands corresponding to the peak (high staining level) and valley (low staining level) dose region in MBRT. The area fraction of positive CD11b staining in the peak region was about two times higher than that in the valley region. Average positive staining in three subregions (frontal cortex, hippocampus, and thalamus) was quantified and compared between the 25 Gy-BBRT and 25 Gy-MBRT groups, as shown in Figure 7A. There were no significant differences between the three assessed subregions within the same treatment group. When

compared to the BBRT group, there was a much higher level of activated microglia in the 25 Gy-MBRT group compared to that in the 25 Gy-BBRT group ($p = 0.024$ for the frontal cortex region and hippocampus region, and $p = 0.109$ for the thalamus region). CD11b staining in surviving mice from the 43 Gy-MBRT group showed a similar level of CD-11b positive staining compared to the 25 Gy-BBRT group and lower staining than the 25 Gy-MBRT group.

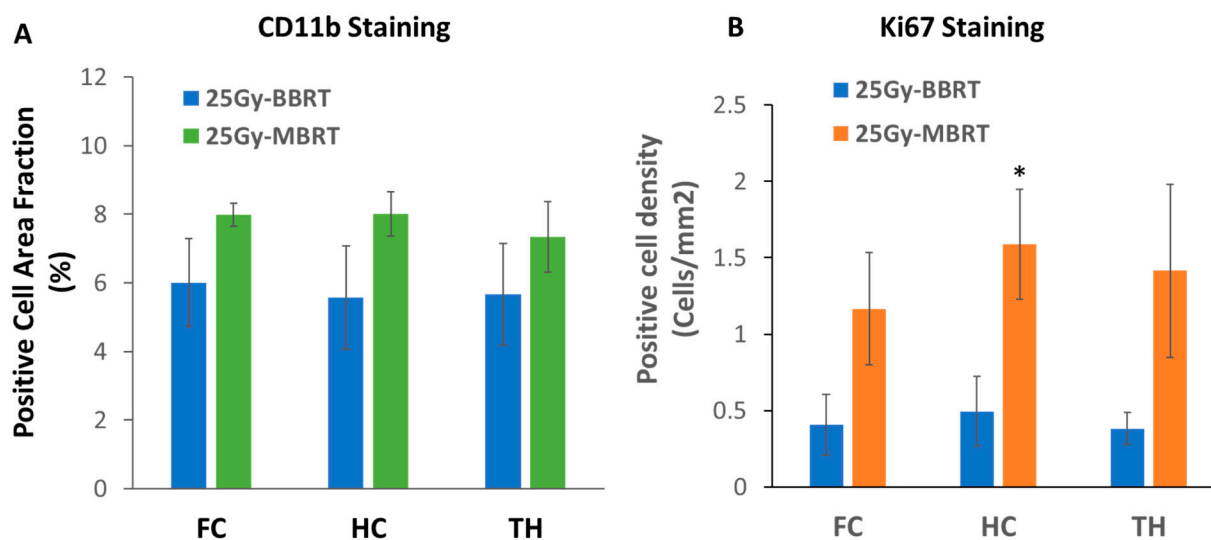


Figure 7. Quantification of CD11b and Ki67 immunostaining in brain tissue at 5 weeks post brain re-irradiation. Area fractions of CD11b (A) and positive Ki67-stained cell density (B) in the frontal cortex (FC), hippocampus (HC), and thalamus (TH) were measured from brain sections collected from 25 Gy-BBRT and 25 Gy-MBRT groups. There was a trend of higher CD11b staining in the MBRT group compared to the BBRT group. No statistical differences were observed ($p > 0.05$). Significantly higher Ki67 staining was shown in the hippocampus of the MBRT group compared to that from the BBRT group ($p = 0.04$), (*) indicates $p < 0.05$.

Cells that are positively stained with Ki67 (Figure 6 lower panel) were considered to be in an active proliferation state, which is indicative of neuroprogenitor cells active for tissue repair. The number of Ki67-positive cells was quantified in the frontal cortex, hippocampal, and thalamus region. As shown in Figure 7B, there was a significantly higher number of Ki67-positive cells in the hippocampus of 25 Gy-MBRT brains compared to that in BBRT brains ($p = 0.04$). Ki67 staining in the frontal cortex and thalamus regions was also higher in the 25 Gy-MBRT group compared to that in the BBRT group, although this was not statistically significant. There was no apparent unevenness to the pattern of Ki67 staining compared to that shown in the CD11b staining of the MBRT treatment group. In the one mouse that survived from 43 Gy-MBRT, the Ki67 staining level was also higher than that from the BBRT group (0.97 vs. 0.49 for the hippocampal region). Statistical comparison was not possible due to the limited number of animals.

4. Discussion

4.1. Potential Benefit from MBRT for Whole-Brain Re-Irradiation

In this pilot study, we investigated the treatment toxicity from re-irradiation using MBRT on normal brains after whole-brain irradiation. We compared gross responses and changes in brain tissue after three different re-irradiation regimens, including conventional uniform irradiation with a dose of 25 Gy, MBRT with the same volume-averaged dose of 25 Gy, and a higher dose of MBRT with the volume-averaged dose of 43 Gy. Mice re-irradiated with 25 Gy of uniform radiation had a significant decrease in average body weight (20% on day 10 and 10% on day 28) after re-irradiation. In contrast, the mean body weight in the 25 Gy-MBRT group did not change significantly on day 10 post-irradiation

and, in fact, increased slightly on day 28 post-irradiation. The immunostaining of brain tissue showed that there was a significantly higher number of proliferating cells (Ki67-positive) in the hippocampus of the 25 Gy-MBRT group compared to the 25 Gy BBRT group. The results showed that, at the same volume average dose, MBRT produced less toxicity than conventional uniform irradiation in whole-brain re-irradiation.

Mice in the 25 Gy-MBRT group had both less body weight loss and a greater number of progenitor cells at 5 weeks after re-irradiation. Body weight is a gross parameter resulting from many radiation-induced CNS tissue/organ responses, including nausea, edema, skin inflammation, fatigue, pain, etc. Progenitor cell preservation or neuronal loss is a local parameter of cellular changes in the CNS after radiation. Both the low weight loss and the preservation of progenitor cells in the 25 Gy-MBRT group suggest less radiation toxicity compared to the BBRT and high-dose MBRT groups. We believe that the reduction in body weight loss indicates less acute toxicity in the 25 Gy-MBRT group. The preservation of progenitor cells in the 25 Gy-MBRT group may be more closely related to the long-term neurological effects. It is possible that the 25 Gy-MBRT group with more preserved progenitor cells may have a lower deficit in neuropsychological function and cognitive ability compared to the BBRT group. It is our interest to study the long-term effects of MBRT in the future.

SFRT has been applied in clinical applications in the form of GRID therapy [11,29] and Lattice therapy [30,31] and in preclinical applications in the form of MRT [13] and MBRT [20]. Both clinical and preclinical studies have a decades-long history demonstrating the superior therapeutic ratio of SFRT with low normal tissue damage compared to conventional radiotherapy [11,32]. Mini-beam radiation as a form of SFRT has been increasingly used in recent years because it is more accessible and feasible for clinical application compared to MRT. The planar mini-beam radiation used in our study had a peak width of 300 μm and a peak-to-peak distance of 1.21 mm. A similar MBRT profile was shown for a normal tissue-sparing effect in our previous reports using single-fraction MBRT treatments [21,33]. In a recent study by Lamirault et al., proton mini-beam radiation (pMBRT) was evaluated for its normal tissue damage in rat models [34]. The pMBRT was delivered with a peak dose of 57 Gy and a valley dose of 8.8 Gy, corresponding to an average volume dose of 25 Gy and a beam width of 0.4 mm with a center-to-center distance of 3.2 mm. The evaluations, which were conducted over a period of 10 months, showed no significant motor or emotional dysfunction in pMBRT-irradiated rats compared to the control animals. Histology analysis also revealed no significant difference between the pMBRT group and the untreated control group. It should be noted that the study did not involve re-irradiation after prior whole-brain irradiation. Data on the normal tissue effects from re-irradiation using MBRT are very limited. Our study is the first to demonstrate the lower toxicity from re-irradiation with MBRT compared to conventional radiation.

4.2. The Role of Valley Dose and Peak Dose in Re-Irradiation Toxicity

We considered several factors in determining the dose level used in this study. The 25 Gy-MBRT group was designed to have the same volume-averaged dose (25 Gy) as that used in the conventional uniform radiation group. This allowed us to compare the two radiation regimens with the same total radiation dose deposition in the brain tissue, with the only variable being the spatial fractionation of the radiation. The 43 Gy-MBRT group was designed to have a valley dose of 15 Gy. In our recent preclinical study on the correlation of SFRT dosimetric parameters and the treatment response using a rat soft tissue sarcoma tumor model, we systematically investigated how each of the eight SFRT dosimetric parameters analyzed was correlated with treatment response (survival, tumor control, and animal body weight change, an indication of treatment toxicity) [20]. The study indicated that a valley dose, rather than a peak dose or a volume-averaged dose, has a strong correlation with tumor control/survival and body weight change. Several studies have also pointed out the importance of the valley dose and the locations of the reservoirs of reparative cells for normal brain toxicity and advised keeping the valley dose

within the known normal tissue tolerance threshold from conventional uniform radiation therapy [27,28,35]. Thus, the valley dose may play an important role in determining the maximum tolerated dose in MBRT. However, it is unknown whether the above hypothesis applies to re-irradiation.

We asked the question of whether the above observation about the importance of the valley dose holds true for whole-brain re-irradiation. We used two MBRT volume-averaged dose levels of 25 Gy and 43 Gy, with corresponding peak/valley doses (at 5 mm depth) of 106 Gy/8.8 Gy and 182 Gy/15.1 Gy (see Table 1). We confirmed that 25 Gy-MBRT with an 8.8 Gy valley dose resulted in less toxicity than the 25 Gy uniform dose BBRT for brain re-irradiation treatment. However, the 43 Gy-MBRT with a 15 Gy valley dose, which is 40% lower than the dose (25 Gy) in the BBRT group, resulted in higher toxicity than 25 Gy-BBRT in the re-irradiation study. This pilot study has shown that for brain re-irradiation, the valley dose or minimum dose affects treatment toxicity differently than SFRT treatment alone. Specifically, the MBRT with the 15 Gy valley dose group (i.e., 43 Gy-MBRT) has dramatically worse survival than the 25 Gy-BBRT and the 25 Gy-MBRT groups. This finding indicates that for re-irradiation application, the clinical significance of the valley dose is different from that in primary SFRT treatment. Other dosimetric parameters, including the peak dose, peak-to-valley distance ratio, peak-to-valley dose ratio, and not just valley dose, may contribute to the overall treatment toxicity. In addition, the brain tolerance valley dose from SFRT may be significantly lower than the tolerance dose of uniform radiation in re-irradiation treatment.

When comparing the two MBRT groups, our results suggested dose-dependent radiation toxicity. The specific mechanisms contributing to the dose-dependent toxicity are far from clear, especially in the case of re-irradiation. It is not clear what is the tolerable peak or valley dose threshold and what is the radiobiological dose response specific to each dosimetric parameter. Is the contribution between the peak and valley dose equal, or are there different weights? Preclinical studies with microbeam radiotherapy (MRT) have shown that animals can tolerate multiple beam arrays with peak doses of 320–860 Gy and beam sizes of 25 to 75 μm , as long as the valley dose is kept below 20 Gy [36–38]. This was not the case in our study. As shown above, the 43 Gy-MBRT with a 15 Gy valley dose was not tolerated in most mice after re-irradiation. In vivo studies with more MBRT dose levels are needed to evaluate dose dependence and to determine which parameter or combination is the most dominant factor in radiation toxicity during re-irradiation.

4.3. Neuroinflammation from MBRT and BBRT Whole-Brain Re-Irradiation

There was a significant amount of CD11b-stained active microglia in both BBRT and 25 Gy-MBRT groups, with a slightly higher area fraction of CD11b in the 25 Gy-MBRT group. In addition, CD11b staining in the MBRT group showed high staining in the peak region and low staining in the valley region, indicating that the neuroinflammation is dose-dependent. CD11b staining has been widely used to label macrophages and activated microglia. Chiang et al. reported that the radiation-induced microglial response in mouse brains and the gliosis were dose-dependent [39]. Moravian et al. investigated the time course of radiation-induced neuroinflammation and reported that increased microglial and T-cell infiltration can be observed for days to months after radiation, leading to long-term brain damage at a high dose of radiation [40]. However, most published studies have focused on initial whole-brain radiation. Our study demonstrated the elevated microglia at 5 weeks post-re-irradiation, indicating the potential long-term tissue damage that might be related to neurocognitive disorders. On the other hand, activated microglia after re-irradiation are expected to be associated with tissue remodeling. Microglia exert various effects on brain development and homeostasis, including neurogenesis, the phagocytosis of dying or apoptotic neurons, synaptic pruning, and myelinogenesis [41]. It would be interesting to conduct a longitudinal study to assess whether the activation of microglia reduces over time and whether there is a difference in the rate of recovery between the BBRT and MBRT groups.

In addition, our study also showed that there was a higher amount of progenitor cells in 25 Gy-MBRT compared to the uniform radiation group. The preservation of progenitor cells in the 25 Gy-MBRT group might be more related to the long-term neurological protection effects. Dilmanian and colleagues applied MBRT to rat spinal cords, which resulted in a loss of oligodendrocytes, astrocytes, and myelin 2 weeks after exposure. But, by 3 months, repopulation and remyelination were nearly complete, suggesting the capacity of recovery from preserved progenitor cells [42]. It is possible that the preserved progenitor cells in the 25 Gy-MBRT group could expedite normal tissue repair and lead to fewer deficits in neuropsychological function and cognition ability in the 25 Gy-BMRT group compared to the BBRT group at later stages.

The biological mechanisms underlying the MBRT-related brain tissue-sparing effects are beyond the neuroinflammation and preservation of progenitor cells. The earlier study with MRT showed that vasculature responded differently in MRT compared to the uniform radiation [43]. The use of a chick chorioallantoic membrane at different stages of development showed that the damages induced by microbeams depended on vessel maturation, and vasculature in normal tissue can recover much better than the vessels in tumor tissue [44]. Vasculature response to MBRT needs to be investigated in the re-irradiation condition. Bystander and abscopal effects from radiation could also play important roles in normal tissue tolerance and tumor inhibition in spatially fractionated radiation treatment [45]. Our study is only an initial step towards exploring the utility of SFRT in whole-brain re-irradiation. More studies are needed to elucidate the working mechanisms and optimal dosimetry in its application for brain re-irradiation.

4.4. Study Limitations

There are several limitations in this pilot study. There was no real-time imaging guidance used in the radiation treatments. Our remedy for the lack of imaging technology included the use of anatomical markers (ears, eyes, and midline), treatment verification film (taped to the mouse skin at the beam entrance to monitor the radiation beam's location and potential animal motion during treatment), radiation light field and real-time video-based animal alignment, and removal from the study of animals whose treatment verification films showed radiation misalignment or motion blur (none occurred in this study).

Another limitation was that only a one-time point, 5 weeks post-re-radiation, was used for the assessment. Radiation responses occurred during and after radiation treatment, and tissue responses could be acute in the early phase of the post-radiation period. Neuroinflammation indicated by leucocyte recruitment can be detected as early as a few hours after radiation [46]. We are aware that these early events could have a major impact on the delayed symptoms of treatment toxicity. And the dynamics and mechanisms of the early tissue responses could be very different between BBRT and MBRT treatments. We believe that the tissue status at a later time point (5 weeks) after brain re-irradiation is less dynamic and is, therefore, a reasonable assessment point for a robust comparison between the two re-irradiation regimens. Future studies with more time points at a long-term stage (months after radiation) are needed to better understand the tissue responses to different brain re-irradiation regimens.

The number of animals in this pilot study was limited. This study provided valuable information and prepared us for a large study with a larger number of animals to evaluate the approach and potential benefits of whole-brain re-irradiation using MBRT.

5. Conclusions

Our pilot study showed that for whole-brain re-irradiation, MBRT with a volume-averaged dose of 25 Gy (peak/valley dose: 106 Gy/8.8 Gy) but not the MBRT with a volume-averaged dose of 43 Gy (peak/valley dose: 182 Gy/15.1 Gy), is less toxic than the 25 Gy of conventional uniform radiation. Immunostaining showed high levels of activated microglial cells in both the BBRT and MBRT groups. And there were more preserved progenitor cells in the 25 Gy-MBRT group compared with the 25 Gy-BBRT group,

indicating the greater potential for tissue repair in the 25 Gy-MBRT group. Our study demonstrates that mini-beam radiation has the potential to provide less toxic whole-brain re-irradiation and warrants further investigation of its application in brain metastases.

Author Contributions: Conceptualization, H.Y., S.X.C. and C.S.; Formal analysis, H.Y., J.N.R. and J.N.; Funding acquisition, H.Y. and C.S.; Methodology, H.Y., J.N.R., J.E.F. and J.N.; Supervision, H.Y. and S.X.C.; Writing—original draft, H.Y. and J.N.R.; Writing—review and editing, H.Y., C.S. and S.X.C. All authors have read and agreed to the published version of the manuscript.

Funding: This research received no external funding.

Institutional Review Board Statement: All animal procedures were approved by the Institutional Animal Care and Use Committee (IACUC) at University of North Carolina at Chapel Hill (Protocol # 22-112).

Informed Consent Statement: Not applicable.

Data Availability Statement: The data presented in this study are available on request from the corresponding authors.

Acknowledgments: The authors thank the Pathology Services Core at UNC Chapel Hill to provide histopathology, immunostaining, and digital scanning services, which is supported in part by the NCI Center Core Support Grant (P30CA016086). We also would like to thank Winnie Tzu-Wen Wang in the Animal MRI core at UNC Chapel Hill who provided animal MRI services.

Conflicts of Interest: The authors declare that they have no conflicts of interest.

References

- Ahluwalia, M.S.; Vogelbaum, M.V.; Chao, S.T.; Mehta, M.M. Brain metastasis and treatment. *F1000Prime Rep.* **2014**, *6*, 114. [[CrossRef](#)]
- Lin, X.; DeAngelis, L.M. Treatment of Brain Metastases. *J. Clin. Oncol.* **2015**, *33*, 3475–3484. [[CrossRef](#)] [[PubMed](#)]
- Johung, K.L.; Yeh, N.; Desai, N.B.; Williams, T.M.; Lautenschlaeger, T.; Arvold, N.D.; Ning, M.S.; Attia, A.; Lovly, C.M.; Goldberg, S.; et al. Extended Survival and Prognostic Factors for Patients With ALK-Rearranged Non-Small-Cell Lung Cancer and Brain Metastasis. *J. Clin. Oncol.* **2016**, *34*, 123–129. [[CrossRef](#)] [[PubMed](#)]
- Sperduto, P.W.; Kased, N.; Roberge, D.; Xu, Z.; Shanley, R.; Luo, X.; Sneed, P.K.; Chao, S.T.; Weil, R.J.; Suh, J.; et al. Effect of tumor subtype on survival and the graded prognostic assessment for patients with breast cancer and brain metastases. *Int. J. Radiat. Oncol. Biol. Phys.* **2012**, *82*, 2111–2117. [[CrossRef](#)] [[PubMed](#)]
- Brown, P.D.; Ahluwalia, M.S.; Khan, O.H.; Asher, A.L.; Wefel, J.S.; Gondi, V. Whole-Brain Radiotherapy for Brain Metastases: Evolution or Revolution? *J. Clin. Oncol.* **2018**, *36*, 483–491. [[CrossRef](#)] [[PubMed](#)]
- Wong, W.W.; Schild, S.E.; Sawyer, T.E.; Shaw, E.G. Analysis of outcome in patients reirradiated for brain metastases. *Int. J. Radiat. Oncol. Biol. Phys.* **1996**, *34*, 585–590. [[CrossRef](#)] [[PubMed](#)]
- Cooper, J.S.; Steinfeld, A.D.; Lerch, I.A. Cerebral metastases: Value of reirradiation in selected patients. *Radiology* **1990**, *174*, 883–885. [[CrossRef](#)] [[PubMed](#)]
- Sadikov, E.; Bezjak, A.; Yi, Q.L.; Wells, W.; Dawson, L.; Millar, B.A.; Laperriere, N. Value of whole brain re-irradiation for brain metastases—single centre experience. *Clin. Oncol.* **2007**, *19*, 532–538. [[CrossRef](#)] [[PubMed](#)]
- Guo, S.; Balagamwala, E.H.; Reddy, C.; Elson, P.; Suh, J.H.; Chao, S.T. Clinical and Radiographic Outcomes From Repeat Whole-brain Radiation Therapy for Brain Metastases in the Age of Stereotactic Radiosurgery. *Am. J. Clin. Oncol.* **2016**, *39*, 288–293. [[CrossRef](#)] [[PubMed](#)]
- Chidambaram, S.; Pannullo, S.C.; Schwartz, T.H.; Wernicke, A.G. Reirradiation of Recurrent Brain Metastases: Where Do We Stand? *World Neurosurg.* **2019**, *125*, 156–163. [[CrossRef](#)]
- Schultke, E.; Balosso, J.; Breslin, T.; Cavaletti, G.; Djonov, V.; Esteve, F.; Grotzer, M.; Hildebrandt, G.; Valdman, A.; Laissue, J. Microbeam radiation therapy—Grid therapy and beyond: A clinical perspective. *Br. J. Radiol.* **2017**, *90*, 20170073. [[CrossRef](#)] [[PubMed](#)]
- Neuner, G.; Mohiuddin, M.M.; Vander Walde, N.; Goloubeva, O.; Ha, J.; Yu, C.X.; Regine, W.F. High-dose spatially fractionated GRID radiation therapy (SFGRT): A comparison of treatment outcomes with Cerrobend vs. MLC SFGRT. *Int. J. Radiat. Oncol. Biol. Phys.* **2012**, *82*, 1642–1649. [[CrossRef](#)] [[PubMed](#)]
- Eling, L.; Bouchet, A.; Nemoz, C.; Djonov, V.; Balosso, J.; Laissue, J.; Brauer-Krisch, E.; Adam, J.F.; Serduc, R. Ultra high dose rate Synchrotron Microbeam Radiation Therapy. Preclinical evidence in view of a clinical transfer. *Radiother. Oncol.* **2019**, *139*, 56–61. [[CrossRef](#)]

14. Bouchet, A.; Brauer-Krisch, E.; Prezado, Y.; El Atifi, M.; Rogalev, L.; Le Clec'h, C.; Laissue, J.A.; Pelletier, L.; Le Duc, G. Better Efficacy of Synchrotron Spatially Microfractionated Radiation Therapy Than Uniform Radiation Therapy on Glioma. *Int. J. Radiat. Oncol. Biol. Phys.* **2016**, *95*, 1485–1494. [[CrossRef](#)] [[PubMed](#)]
15. Slatkin, D.N.; Spanne, P.; Dilmanian, F.A.; Gebbers, J.O.; Laissue, J.A. Subacute neuropathological effects of microplanar beams of x-rays from a synchrotron wiggler. *Proc. Natl. Acad. Sci. USA* **1995**, *92*, 8783–8787. [[CrossRef](#)] [[PubMed](#)]
16. Prezado, Y.; Deman, P.; Varlet, P.; Jouvion, G.; Gil, S.; Le Clec, H.C.; Bernard, H.; Le Duc, G.; Sarun, S. Tolerance to Dose Escalation in Minibeam Radiation Therapy Applied to Normal Rat Brain: Long-Term Clinical, Radiological and Histopathological Analysis. *Radiat. Res.* **2015**, *184*, 314–321. [[CrossRef](#)]
17. Prezado, Y.; Sarun, S.; Gil, S.; Deman, P.; Bouchet, A.; Le Duc, G. Increase of lifespan for glioma-bearing rats by using minibeam radiation therapy. *J. Synchrotron. Radiat.* **2012**, *19*, 60–65. [[CrossRef](#)] [[PubMed](#)]
18. Prezado, Y.; Dos Santos, M.; Gonzalez, W.; Jouvion, G.; Guardiola, C.; Heinrich, S.; Labiod, D.; Juchaux, M.; Jourdain, L.; Sebrie, C.; et al. Transfer of Minibeam Radiation Therapy into a cost-effective equipment for radiobiological studies: A proof of concept. *Sci. Rep.* **2017**, *7*, 17295. [[CrossRef](#)] [[PubMed](#)]
19. Bazyar, S.; Inscoc, C.R.; O'Brian, E.T.; Zhou, O.; Lee, Y.Z. Minibeam radiotherapy with small animal irradiators; in vitro and in vivo feasibility studies. *Phys. Med. Biol.* **2017**, *62*, 8924–8942. [[CrossRef](#)] [[PubMed](#)]
20. Rivera, J.N.; Kierski, T.M.; Kasoji, S.K.; Abrantes, A.S.; Dayton, P.A.; Chang, S.X. Conventional dose rate spatially-fractionated radiation therapy (SFRT) treatment response and its association with dosimetric parameters-A preclinical study in a Fischer 344 rat model. *PLoS ONE* **2020**, *15*, e0229053. [[CrossRef](#)]
21. Yuan, H.; Zhang, L.; Frank, J.E.; Inscoc, C.R.; Burk, L.M.; Hadsell, M.; Lee, Y.Z.; Lu, J.; Chang, S.; Zhou, O. Treating Brain Tumor with Microbeam Radiation Generated by a Compact Carbon-Nanotube-Based Irradiator: Initial Radiation Efficacy Study. *Radiat. Res.* **2015**, *184*, 322–333. [[CrossRef](#)]
22. Smart, D. Radiation Toxicity in the Central Nervous System: Mechanisms and Strategies for Injury Reduction. *Semin. Radiat. Oncol.* **2017**, *27*, 332–339. [[CrossRef](#)] [[PubMed](#)]
23. Billena, C.; Khan, A.J. A Current Review of Spatial Fractionation: Back to the Future? *Int. J. Radiat. Oncol. Biol. Phys.* **2019**, *104*, 177–187. [[CrossRef](#)] [[PubMed](#)]
24. Griffin, R.J.; Prise, K.M.; McMahon, S.J.; Zhang, X.; Penagaricano, J.; Butterworth, K.T. History and current perspectives on the biological effects of high-dose spatial fractionation and high dose-rate approaches: GRID, Microbeam & FLASH radiotherapy. *Br. J. Radiol.* **2020**, *93*, 20200217. [[CrossRef](#)] [[PubMed](#)]
25. Yan, W.; Khan, M.K.; Wu, X.; Simone, C.B., 2nd; Fan, J.; Gressen, E.; Zhang, X.; Limoli, C.L.; Bahig, H.; Tubin, S.; et al. Spatially fractionated radiation therapy: History, present and the future. *Clin. Transl. Radiat. Oncol.* **2020**, *20*, 30–38. [[CrossRef](#)] [[PubMed](#)]
26. Trappetti, V.; Fazzari, J.M.; Fernandez-Palomo, C.; Scheidegger, M.; Volarevic, V.; Martin, O.A.; Djonov, V.G. Microbeam Radiotherapy-A Novel Therapeutic Approach to Overcome Radioresistance and Enhance Anti-Tumour Response in Melanoma. *Int. J. Mol. Sci.* **2021**, *22*, 7755. [[CrossRef](#)] [[PubMed](#)]
27. Dilmanian, F.A.; Button, T.M.; Le Duc, G.; Zhong, N.; Pena, L.A.; Smith, J.A.; Martinez, S.R.; Bacarian, T.; Tammam, J.; Ren, B.; et al. Response of rat intracranial 9L gliosarcoma to microbeam radiation therapy. *Neuro-Oncol.* **2002**, *4*, 26–38. [[CrossRef](#)]
28. Laissue, J.A.; Bartzsch, S.; Blattmann, H.; Brauer-Krisch, E.; Bravin, A.; Dallery, D.; Djonov, V.; Hanson, A.L.; Hopewell, J.W.; Kaser-Hotz, B.; et al. Response of the rat spinal cord to X-ray microbeams. *Radiother. Oncol.* **2013**, *106*, 106–111. [[CrossRef](#)] [[PubMed](#)]
29. Laissue, J.A.; Blattmann, H.; Slatkin, D.N. Alban Kohler (1874–1947): Inventor of grid therapy. *Z. Fur Med. Phys.* **2012**, *22*, 90–99. [[CrossRef](#)]
30. Zhang, H.; Wu, X.; Zhang, X.; Chang, S.X.; Megooni, A.; Donnelly, E.D.; Ahmed, M.M.; Griffin, R.J.; Welsh, J.S.; Simone, C.B., 2nd; et al. Photon GRID Radiation Therapy: A Physics and Dosimetry White Paper from the Radiosurgery Society (RSS) GRID/LATTICE, Microbeam and FLASH Radiotherapy Working Group. *Radiat. Res.* **2020**, *194*, 665–677. [[CrossRef](#)]
31. Wu, X.; Perez, N.C.; Zheng, Y.; Li, X.; Jiang, L.; Amendola, B.E.; Xu, B.; Mayr, N.A.; Lu, J.J.; Hatoum, G.F.; et al. The Technical and Clinical Implementation of LATTICE Radiation Therapy (LRT). *Radiat. Res.* **2020**, *194*, 737–746. [[CrossRef](#)] [[PubMed](#)]
32. Fernandez-Palomo, C.; Fazzari, J.; Trappetti, V.; Smyth, L.; Janka, H.; Laissue, J.; Djonov, V. Animal Models in Microbeam Radiation Therapy: A Scoping Review. *Cancers* **2020**, *12*, 527. [[CrossRef](#)] [[PubMed](#)]
33. Zhang, L.; Yuan, H.; Burk, L.M.; Inscoc, C.R.; Hadsell, M.J.; Chtcheprov, P.; Lee, Y.Z.; Lu, J.; Chang, S.; Zhou, O. Image-guided microbeam irradiation to brain tumour bearing mice using a carbon nanotube x-ray source array. *Phys. Med. Biol.* **2014**, *59*, 1283–1303. [[CrossRef](#)] [[PubMed](#)]
34. Lamirault, C.; Doyere, V.; Juchaux, M.; Pouzoulet, F.; Labiod, D.; Dendale, R.; Patriarca, A.; Nauraye, C.; Le Dudal, M.; Jouvion, G.; et al. Short and long-term evaluation of the impact of proton minibeam radiation therapy on motor, emotional and cognitive functions. *Sci. Rep.* **2020**, *10*, 13511. [[CrossRef](#)] [[PubMed](#)]
35. Mukumoto, N.; Nakayama, M.; Akasaka, H.; Shimizu, Y.; Osuga, S.; Miyawaki, D.; Yoshida, K.; Ejima, Y.; Miura, Y.; Umetani, K.; et al. Sparing of tissue by using micro-slit-beam radiation therapy reduces neurotoxicity compared with broad-beam radiation therapy. *J. Radiat. Res.* **2017**, *58*, 17–23. [[CrossRef](#)] [[PubMed](#)]
36. Brauer-Krisch, E.; Requardt, H.; Regnard, P.; Corde, S.; Siegbahn, E.; LeDuc, G.; Brochard, T.; Blattmann, H.; Laissue, J.; Bravin, A. New irradiation geometry for microbeam radiation therapy. *Phys. Med. Biol.* **2005**, *50*, 3103–3111. [[CrossRef](#)] [[PubMed](#)]

37. Bouchet, A.; Lemasson, B.; Le Duc, G.; Maisin, C.; Brauer-Krisch, E.; Siegbahn, E.A.; Renaud, L.; Khalil, E.; Remy, C.; Poillot, C.; et al. Preferential effect of synchrotron microbeam radiation therapy on intracerebral 9L gliosarcoma vascular networks. *Int. J. Radiat. Oncol. Biol. Phys.* **2010**, *78*, 1503–1512. [[CrossRef](#)] [[PubMed](#)]
38. Fukunaga, H.; Butterworth, K.T.; McMahon, S.J.; Prise, K.M. A Brief Overview of the Preclinical and Clinical Radiobiology of Microbeam Radiotherapy. *Clin. Oncol.* **2021**, *33*, 705–712. [[CrossRef](#)] [[PubMed](#)]
39. Chiang, C.S.; McBride, W.H.; Withers, H.R. Radiation-induced astrocytic and microglial responses in mouse brain. *Radiother. Oncol.* **1993**, *29*, 60–68. [[CrossRef](#)] [[PubMed](#)]
40. Moravan, M.J.; Olschowka, J.A.; Williams, J.P.; O'Banion, M.K. Cranial irradiation leads to acute and persistent neuroinflammation with delayed increases in T-cell infiltration and CD11c expression in C57BL/6 mouse brain. *Radiat. Res.* **2011**, *176*, 459–473. [[CrossRef](#)]
41. Liu, Q.; Huang, Y.; Duan, M.; Yang, Q.; Ren, B.; Tang, F. Microglia as Therapeutic Target for Radiation-Induced Brain Injury. *Int. J. Mol. Sci.* **2022**, *23*, 8286. [[CrossRef](#)] [[PubMed](#)]
42. Dilmanian, F.A.; Qu, Y.; Feinendegen, L.E.; Pena, L.A.; Bacarian, T.; Henn, F.A.; Kalef-Ezra, J.; Liu, S.; Zhong, Z.; McDonald, J.W. Tissue-sparing effect of x-ray microplanar beams particularly in the CNS: Is a bystander effect involved? *Exp. Hematol.* **2007**, *35*, 69–77. [[CrossRef](#)] [[PubMed](#)]
43. Brauer-Krisch, E.; Serduc, R.; Siegbahn, E.; Le Duc, G.; Prezado, Y.; Bravin, A.; Blattmann, H.; Laissue, J. Effects of pulsed, spatially fractionated, microscopic synchrotron X-ray beams on normal and tumoral brain tissue. *Mutat. Res.* **2010**, *704*, 160–166. [[CrossRef](#)] [[PubMed](#)]
44. Bouchet, A.; Serduc, R.; Laissue, J.A.; Djonov, V. Effects of microbeam radiation therapy on normal and tumoral blood vessels. *Phys. Med.* **2015**, *31*, 634–641. [[CrossRef](#)] [[PubMed](#)]
45. Wu, J.; Hei, T.K. Focus small to find big—The microbeam story. *Int. J. Radiat. Biol.* **2018**, *94*, 782–788. [[CrossRef](#)] [[PubMed](#)]
46. Yuan, H.; Goetz, D.J.; Gaber, M.W.; Issekutz, A.C.; Merchant, T.E.; Kiani, M.F. Radiation-induced up-regulation of adhesion molecules in brain microvasculature and their modulation by dexamethasone. *Radiat. Res.* **2005**, *163*, 544–551. [[CrossRef](#)]

Disclaimer/Publisher's Note: The statements, opinions and data contained in all publications are solely those of the individual author(s) and contributor(s) and not of MDPI and/or the editor(s). MDPI and/or the editor(s) disclaim responsibility for any injury to people or property resulting from any ideas, methods, instructions or products referred to in the content.